Bull. Mater. Sci., Vol. 36, No. 7, December 2013, pp. 1297–1306. © Indian Academy of Sciences.

Structural characterization and complex impedance studies on fast ion conducting mixed system $(SbI_3)_x$–$(Ag_2CrO_4)_{1-x}$

S AUSTIN SUTHANTHIRARAJ[*] **and S SAROJINI**[†]

Department of Energy, University of Madras, Guindy Campus, Chennai 600 025, India
[†]PG and Research Department of Physics, Queen Mary's College, Chennai 600 004, India

MS received 15 July 2012; revised 18 February 2013

Abstract. **This paper deals with preparation and physico-chemical characterization of a new mixed system, $(SbI_3)_x$–$(Ag_2CrO_4)_{1-x}$ ($0{\cdot}1 \leq x \leq 0{\cdot}9$), undertaken with a view to evaluate silver ion transport properties and identify those fast ion conducting compositions. Polycrystalline samples of various compositions were synthesized by rapid melt-quenching method. Powder X-ray diffraction (XRD) analysis in conjunction with differential scanning calorimetry (DSC) and electrical transport evaluation involving silver ionic transport number and temperature-dependent electrical complex impedance measurements were carried out in order to identify the different phases responsible for the conduction mechanism. Realization of a fast ionic conductivity value of $3{\cdot}2 \times 10^{-2}$ S cm^{-1} in the case of the composition, $(SbI_3)_{0.3}$–$(Ag_2CrO_4)_{0.7}$, at room temperature due to silver ion transport has been discussed in terms of observed structural and thermal characteristics. A detailed analysis of conductivity spectra pertaining to the best conducting system, $(SbI_3)_{0.3}$–$(Ag_2CrO_4)_{0.7}$, has also been presented.**

Keywords. **Electrical conductivity; impedance; DSC; XRD; conductivity spectra.**

1. Introduction

In the realm of modern materials research involving new materials, solid state devices appear to be significant to our economies and fascinating too. For instance, remarkable interest witnessed over the past few decades in solid electrolytes or fast ionic systems stems from their device applications in solid state batteries, fuel cells, sensors and so on. Fast ion conducting glasses exhibit certain advantages over their crystalline counterparts owing to their isotropic properties, ease of formation and tailor-made properties with a desired change in composition. Silver iodide which is one of the well known fast ionic conducting solid exists in three polymorphic forms as α (bcc), β (wurtzite) and γ (zincblende) wherein α is stable above 420 K, is the fast ionic phase, which has been extensively studied (Patnaik and Sunandana 1998). However, α-AgI is thermodynamically stable only in the temperature range between 420 and 828 K and β and γ-AgI are the stable phases at temperatures lower than 420 K. The conductivities of β or γ-AgI are as low as about 10^{-5} S cm^{-1} at room temperature. Various techniques have been employed to achieve fast ionic conduction at room temperature in AgI-based systems either by adding second components to AgI to form new compounds such as Ag_3SI and $RbAg_4I_5$ or by adding various kinds of silver oxysalts to form superionic conducting solids (Saito *et al* 1993). Literature references in the field of fast ion conducting systems over the past three decades portrays AgI-based fast ionic systems as promising candidates possessing ionic conductivities in the order of 10^{-3}–10^{-1} S cm^{-1} at room temperature (Chandra 1981; Minami 1983; Kanchan *et al* 2004; Bhattacharya and Ghosh 2005; Nowinski *et al* 2007; Veeranna Gowda and Anavekar 2007). A highly disordered structure is an essential feature for the superionic conductors in view of their applications to solid-state ionic devices and also thorough comparative investigation of thermal and other properties of these amorphous superionic conductors is highly desirable particularly the glass transition and crystallization kinetic studies. In the isothermal crystallization kinetics, the temperature is kept constant whereas in non isothermal measurements the DSC experiments are performed at different heating rates. Both the techniques lead to determination of thermodynamic parameters such as glass (T_g) and amorphous $\leftrightarrow$ crystalline transition (T_c) temperatures and the corresponding enthalpy and entropy changes (ΔH and ΔS, respectively), activation energies for structural relaxation (E_s) and crystallization (E_c), and the order parameter (n) (Dalvi *et al* 2005).

In order to arrive at new series of fast ionic systems in a cost-effective manner, researchers in the recent past replaced AgI with other metal halides such as CdI_2, CuI, ZnI_2, PbI_2 and alkali halides like NaI or KI (Viswanathan and Suthanthiraraj 1992, 1993; Suthanthiraraj *et al* 2001; Padmasree *et al* 2005; Suthanthiraraj and Vinod Mathew 2005) resulting in electrical conductivities comparable to that of their AgI-based counterparts. On the other hand, the presence of certain cations such as Cs^+, Cu^+, Zn^{2+}, Pb^{2+} or

[*]Author for correspondence (suthan98@gmail.com)

Sb^{3+} ion led to possible coordination with the oxygen ion within the oxyanion framework thereby facilitating easy conduction pathways for Ag^+ ions to move towards an iodine-rich environment (El Damrawi *et al* 2000; Renard *et al* 2002) and the role of silver oxysalt Ag_2CrO_4 in forming glassy networks has already been well established in the literature (Viswanathan and Suthanthiraraj 1992; Durga Rani and Hariharan 1996). The present work has been undertaken with an aim of arriving at a family of silver ion conducting fast ionic solids by appropriately substituting antimony iodide, SbI_3 for AgI into the network of a typical silver oxysalt, viz. silver chromate Ag_2CrO_4 in order to form a new mixed system, SbI_3–Ag_2CrO_4 and understanding their structural, thermal and electrical characteristics.

2. Experimental

2.1 *Sample preparation*

Some of the widely used preparation techniques include melt quenching, flash evaporation, sol–gel process etc. In the preparation of solids, usually special care has to be taken to use proper stoichiometric quantities, pure starting materials and to ensure that the reaction is completed because it is usually not possible to purify a solid once it has been formed. The method chosen for any solid will depend not only on the composition of the solid but also on the form it is required for its proposed use. In the melt-quenching method, the raw materials are melted above the melting point and then rapidly quenched with liquid nitrogen. To achieve a homogeneous mix of small particles, it is necessary to be very thorough in grinding the reactants. Hence, all the starting materials are ground well to attain a small particle size, and hence are very well mixed to maximize the surface contact area and minimize the distance that the reactants have to diffuse. Evacuated tubes are employed when products or reactants are sensitive to air or water or are volatile. Depending on the temperature of reaction, Pyrex or silica (quartz) are the common choices for such reaction tubes, as they are fairly inert, and may be sealed using vacuum system for easy handling. One of the benefits of the melt-quench technique is that the resultant solid material from a high quenching rate is chemically homogenous and therefore, it is possible to obtain different shapes and forms which may be the desired characteristic in device applications.

In the present investigation, the conventional melt-quenching technique involving vacuum-sealed quartz tubes has been employed in order to prevent the starting materials from reacting with atmospheric oxygen and hence forming any impurity compounds. Moreover, this technique averts the possibility of the resultant melt seeping into the semi-porous boat at high temperatures as generally found in the case of open-air ceramic boat-quenching technique, thus leading to a reduction in the yield of the final product. Accordingly, analar grade chemicals of antimony iodide, SbI_3 and silver chromate, Ag_2CrO_4, were used as raw materials for the synthesis of different compositions of the chosen binary system, $(SbI_3)_x$–$(Ag_2CrO_4)_{1-x}$, where $x = 0{\cdot}9$, $0{\cdot}8$, $0{\cdot}7$, $0{\cdot}6$, $0{\cdot}5$, $0{\cdot}4$, $0{\cdot}3$, $0{\cdot}2$ and $0{\cdot}1$ mole fraction, respectively by annealing mixtures of appropriate amounts of the starting materials in a vacuum-sealed quartz ampoule kept over a ceramic boat at 873 K for 6 h in a high temperature furnace and rapidly quenching the molten mixture in a liquid nitrogen bath. The resultant products were finely powdered using a pestle and mortar and stored in a darkened desiccator for further investigation.

2.2 *Powder X-ray diffraction*

X-ray diffraction (XRD) measurements were carried out on all the powdered samples of the mixed system, $(SbI_3)_x$–$(Ag_2CrO_4)_{1-x}$, where $x = 0{\cdot}9, 0{\cdot}8, 0{\cdot}7, 0{\cdot}6, 0{\cdot}5, 0{\cdot}4, 0{\cdot}3, 0{\cdot}2$ and $0{\cdot}1$ mole fraction, respectively at room temperature using a Siefert X-ray Diffractometer with CuKα_1 radiation ($\lambda = 1.541$ Å).

2.3 *Differential scanning calorimetry*

The thermal events were recorded for all the specimens of the system, $(SbI_3)_x$–$(Ag_2CrO_4)_{1-x}$,$(0{\cdot}1 \leq x \leq 0{\cdot}9)$, in the temperature range of 323–573 K using a Perkin Elmer model DSC-7 differential scanning calorimeter at a heating rate of 20 K min^{-1} with platinum as the reference material and aluminum sample containers.

2.4 *Complex impedance analysis*

The freshly-prepared solid samples of the mixed system, $(SbI_3)_x$–$(Ag_2CrO_4)_{1-x}$ $(0{\cdot}1 \leq x \leq 0{\cdot}9)$, were ground and pressed together with appropriate silver electrodes on both sides under a pelletizing pressure of 5 ton cm^{-2} in order to make circular pellets of 8 mm diameter. These electrodes comprised of metallic silver powder and sample mixed in the weight ratio of 2:1. Any metallic electrode which is different from the components of the mixed conductors may be used as an ion blocking electrode or as a non-blocking electrode. For example, Pt electrodes were used as ion blocking electrodes for electronic conductivity measurements in oxide ion electrolytes in d.c. method (Ahn *et al* 2011). Similarly, Au electrodes were used as non-blocking electrodes in order to enhance electronic conductivity.

In the case of yttria-stabilized zirconia (YSZ), choice of electrode metal has a significant influence on the electrode properties with Ag as the best and Au as the poorest. Hence, the respective electrode resistance values could be ranked by $R_{Ag} < R_{Au} < R_{Pt}$, with $R_{Au} \sim 10^2 - 10^3 \times R_{Pt}$. On the other hand, for the stabilized δ-bismuth sesqui-oxides, in particular, $(Bi_2O_3)_{0{\cdot}75}(Er_2O_3)_{0{\cdot}25}$ (abbreviated as BiEr25), there is very little difference in performance between Pt and Au electrodes with similar electrode morphology. In the case of $Bi_2Cu_{0{\cdot}1}V_{0{\cdot}9}O_{5{\cdot}35}$ system, similar trend was observed

in the performance of Au, Pt and Ag electrode metals (Boukamp 2000).

The complex impedance measurements were carried out using a computer-controlled Hewlett-Packard model HP4284A Precision LCR Meter in the frequency range of 20 Hz–1 MHz over the temperature region 298–435 K. Essentially, the frequency response of the sample under analysis could be represented by an equivalent circuit consisting of a parallel combination of circuit elements, R_b and C_g, denoting the bulk resistance and geometric capacitance, respectively, whereas the resultant intercept of the semicircular arcs of impedance plot (i.e. plot of Z'' vs Z' where Z' and Z'' denote the real and imaginary parts of the complex impedance Z^*) on the real axis would indicate the bulk resistance, R_b, of the specimen. A schematic representation of a fast ionic solid sandwiched between two non-blocking (i.e. reversible silver) electrodes together with the relevant equivalent circuit and impedance plot is shown in figure 1 (Macdonald 1973, 1974, 1987; Suthanthiraraj and Mala 2003).

All the observed impedance plots were best fitted internally by means of the Boukamp equivalent circuit software package incorporated within the computer. Equivalent circuits are traditionally used to model a.c. impedance data. An equivalent electrical circuit (EEC) is an electrical circuit with the same impedance spectrum as the experimental data. The values and arrangement of the circuit elements ideally represent physical properties or phenomena. Electrochemical impedance spectroscopy (EIS) is a powerful diagnostic technique that finds extensive use in electrochemistry, especially for the multi-electron transfer processes. Combinations of purely resistive, capacitive, or inductive behaviours do not necessarily describe the response of all systems and hence constant phase elements (CPE) are used to model this behaviour (Biendicho and West 2012).

The experimental impedance data were well fitted using the fitting procedure according to Boukamp, by treating various impedance parameters as variables of applied voltage. For each set of experimental data, the parameters of EEC were fitted using the complex nonlinear least square (CNLS) fitting procedure using the Boukamp's equivalent circuit software. The complex nonlinear least squares (CNLS) method is one of the most common approaches for modelling impedance data. CNLS is used to fit real and imaginary parts or the magnitude and phase of experimental impedance or admittance data to an equivalent circuit or a rational function. It is a convenient method for fitting data to functions (Boukamp 1986).

The impedance analyses of the samples were performed by nonlinear least square (NLLS) fitting procedure. NLLS fitting is performed in two steps, in the partial NLLS fit, suitable points are selected in a straight line and part of the impedance data through which a tangential line is drawn. The intersection of the line with the real axis gives the bulk resistance. By choosing a set of three data points in the high frequency depressed semicircle, NLLS fit yields the values for the impedance and CPE parameters. Later, both inclined straight line and semicircle parts are simultaneously fitted to the NLLS fit procedure to yield a set of parameters (e.g. circuit elements) of the equivalent circuit. Thus, performed analysis reduces most of the systematic errors and deduces the parameters for an equivalent circuit. The complex nonlinear least square method centres on minimizing the object function S with respect to the parameters a_k of the model function, $Z(\omega, a_k)$:

$$\sum_{i=1}^{N} w_i\{[Z_{re,i} - Z_{re}(\omega_i, a_k)]^2 + \left[Z_{im,i} - Z_{im}(\omega_i, a_k)\right]^2\}, \tag{1}$$

where $Z_{re,i} + jZ_{im,i}$ represents the measured impedance at frequency, ω_i and w_i the weighed factor. An important control tool is the distribution of the residuals *vs* frequency. For a good match between data and model, the residuals should be randomly distributed around the log ω axis (Boukamp 2004).

The experimental impedance data were well fitted using the fitting procedure according to Boukamp by treating the various impedance parameters as variables of applied voltage. For each set of experimental data, parameters of EEC were fitted using the complex nonlinear least square (CNLS) fitting procedure. The goodness of fit value of χ- quadrate of 10^{-4} or less indicates a reasonably good fit using a minimum number of elements within an error of 5% (Hull *et al* 2002; Metikos *et al* 2003).

Thus, the values of R_b for individual samples at various temperatures could be estimated accurately during the present investigation.

2.5 *Silver ionic transport number measurements*

The electromotive force (EMF) method was employed for the estimation of silver ionic transport number (t_{Ag+}) in each composition of the present system at room temperature. Accordingly, a galvanic cell was fabricated with a configuration

$$(-)\ \mathrm{Ag} + \text{sample/sample/}\mathrm{I_2}(+),$$

where a powder mixture of metallic silver powder and the sample taken in the weight ratio 2:1 was used as anode. The cell components were cascaded and pressed together into a circular pellet at a pelletizing pressure of 5 ton cm^{-2} so as to constitute the galvanic cell. The values of open circuit voltage (E_t), (OCV) of such solid-state electrochemical cells were measured and compared with the thermodynamic value of 687 mV (E_o) reported for the Ag/I_2 couple for arriving at room temperature silver ionic transport number (t_{Ag+}) data corresponding to each composition of the present mixed system (Suthanthiraraj and Mala 2003) where

$$t_{Ag+} = \frac{E_t}{E_o}, \tag{2}$$

and for fast ionic solids with high ionic conductivities, the value of t_{Ag+} is found to be almost unity.

3. Results and discussion

3.1 *Phase identification from XRD data*

The observed room temperature powder X-ray diffraction (XRD) patterns for the set of nine different compositions of the mixed system $(SbI_3)_x$–$(Ag_2CrO_4)_{1-x}$ corresponding to $x = 0{\cdot}9$, $0{\cdot}8$, $0{\cdot}7$, $0{\cdot}6$, $0{\cdot}5$, $0{\cdot}4$, $0{\cdot}3$, $0{\cdot}2$ and $0{\cdot}1$ mole fraction are presented in figure 2(a–i). A careful scrutiny of all XRD peaks was performed by means of XRD analysis software in conjunction with JCDPS diffraction data in order to identify the various phases formed. It is apparent from figure 2 that most of the observed XRD patterns exhibit well-defined peaks indicating the presence of polycrystalline solid materials except the XRD pattern designated as 'g' corresponding to specimen having $x = 0{\cdot}3$ mole fraction, respectively. This implies that all those SbI_3-rich compositions are essentially polycrystalline in nature. The fact that the particular composition containing $x = 0{\cdot}3$ mole fraction has been characterized by broad and very much less intense peaks in XRD pattern tends to suggest the formation of relatively disordered-type of material within this specimen. Interestingly, the occurrence of an intense peak at $2\theta = 26{\cdot}67°$ along with a series of less-intense peaks at $2\theta = 35{\cdot}1$ and $41{\cdot}8°$ in the case of XRD pattern denoted as 'a' may be attributed to the existence of excess or unreacted starting material viz. SbI_3, owing to the presence of characteristic [*h k l*] lines corresponding to [1 1 3], [1 1 6] and [3 0 0] reflections, respectively (JCDPS File no. 740456) considering the richness of SbI_3 in this composition (having 0·9 mole fraction) as compared to Ag_2CrO_4. On the other hand, those patterns represented as 'b' and 'c' in figure 1 show a gradual shift associated with the above reflections, thus suggesting the onset of formation of certain new phases in the case of specimens containing $x = 0{\cdot}8$ and $0{\cdot}7$ mole fraction as a result of probable solid-state reactions occurring between SbI_3 and Ag_2CrO_4. Furthermore, in the present XRD pattern designated as 'd', a set of characteristic peaks corresponding to the presence of AgI cubic phase (space group $F43m$) (JCDPS file no. 780641) are noticed in the form of [*h k l*] lines [1 1 1], [2 2 0] and [3 1 1] at $2\theta = 23{\cdot}7$, $39{\cdot}2$ and $46{\cdot}3°$, respectively thus revealing the formation of AgI as one of the reaction products in this particular composition containing $0 \cdot 6$ mole fraction of SbI_3. Similarly, figure 1 tends to confirm the existence of AgI phase in the case of two consecutive compositions possessing 0·5 and 0·4 mole fractions of SbI_3(i.e. $x = 0{\cdot}5$ and $0{\cdot}4$) owing to the occurrence of intense peaks around $2\theta = 23{\cdot}7$, $39{\cdot}2$ and $46{\cdot}3°$ corresponding to pure AgI in the XRD pattern denoted as 'e' and 'f'. Furthermore, XRD pattern designated as 'f' appears to be less intense compared to the pattern marked as 'e'.

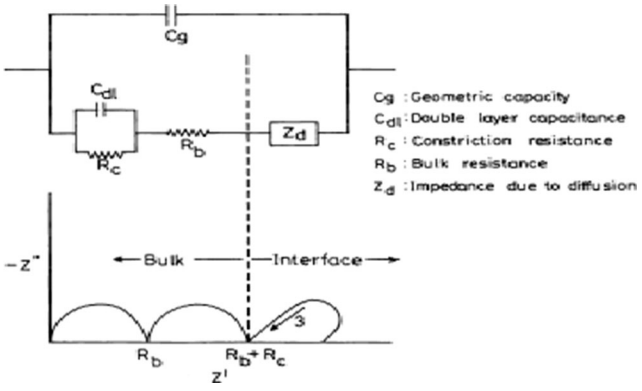

Figure 1. Schematic representation of equivalent circuit and impedance plot.

A careful examination of figure 2 suggests that in the case of compositions corresponding to $x = 0{\cdot}1$ and $0{\cdot}2$ mole fractions, the observed XRD peaks are relatively less intense compared to that of remaining compositions. Typically, the composition having $x = 0{\cdot}1$ mole fraction is found to exhibit a set of three characteristic XRD peaks of AgI at $2\theta = 23{\cdot}7$, $39{\cdot}2$ and $46{\cdot}3°$ ascribable to [*h k l*] planes of [1 1 1], [2 2 0] and [3 1 1], respectively in addition to three peaks at $2\theta = 31{\cdot}1$, $31{\cdot}4$ and $32{\cdot}3°$ owing to the presence of Ag_2CrO_4 in orthorhombic phase (space group, *Pnma*) which may be attributed to [*h k l*] reflection planes of [3 0 1], [1 2 1] and [0 0 2], respectively (JCDPS file no. 780641; JCDPS file no. 720858). In the case of $x = 0{\cdot}2$ mole fraction, it is seen from figure 2 that three characteristic XRD peaks of AgI appear at $2\theta = 23{\cdot}7$, $39{\cdot}2$ and $46{\cdot}3°$ ascribable to [*h k l*] planes of [1 1 1], [2 2 0] and [3 1 1], respectively apart from those three characteristic peaks of $CrSbO_4$ in tetragonal phase (space group, $P4_2/mnm$) observed at $2\theta = 27{\cdot}5$, $35{\cdot}2$ and $53{\cdot}7°$ corresponding to [*h k l*] planes of [1 1 0], [1 0 1] and [2 1 1], respectively (JCDPS file no. 780641; JCPDS file no. 351288). On the other hand, it is interesting to note from figure 1 that less intense peaks corresponding to AgI appear at $2\theta = 23{\cdot}7$, $39{\cdot}2$ and $46{\cdot}3°$ owing to the reflection planes of [1 1 1], [2 2 0] and [3 1 1], respectively in the case of composition having $x = 0{\cdot}3$ mole fraction (JCDPS file no. 780641).The above compositions are thus found to be polycrystalline in nature. The disordered nature of the composition corresponding to $x = 0{\cdot}3$ mole fraction as revealed by the present XRD results appears to suggest that such specimen would be expected to exhibit interesting ion-transport features too, as discussed in the subsequent section.

It is inferred that AgI phase is formed only in certain compositions as one of the constituents wherein favourable experimental conditions exist for possible ion exchange chemical reactions to occur within the molten specimens of the chosen multi-phase system, SbI_3–Ag_2CrO_4 and hopping of Ag^+ ions within the lattice may lead to a highly disordered state which in turn would influence the behaviour of electrical characteristics of those compositions as well.

3.2 *Differential scanning calorimetric analysis*

The differential scanning calorimetric (DSC) traces obtained for the nine different compositions of the mixed system $(SbI_3)_x$–$(Ag_2CrO_4)_{1-x}$, where $x = 0{\cdot}9$, $0{\cdot}8$, $0{\cdot}7$, $0{\cdot}6$, $0{\cdot}5$,

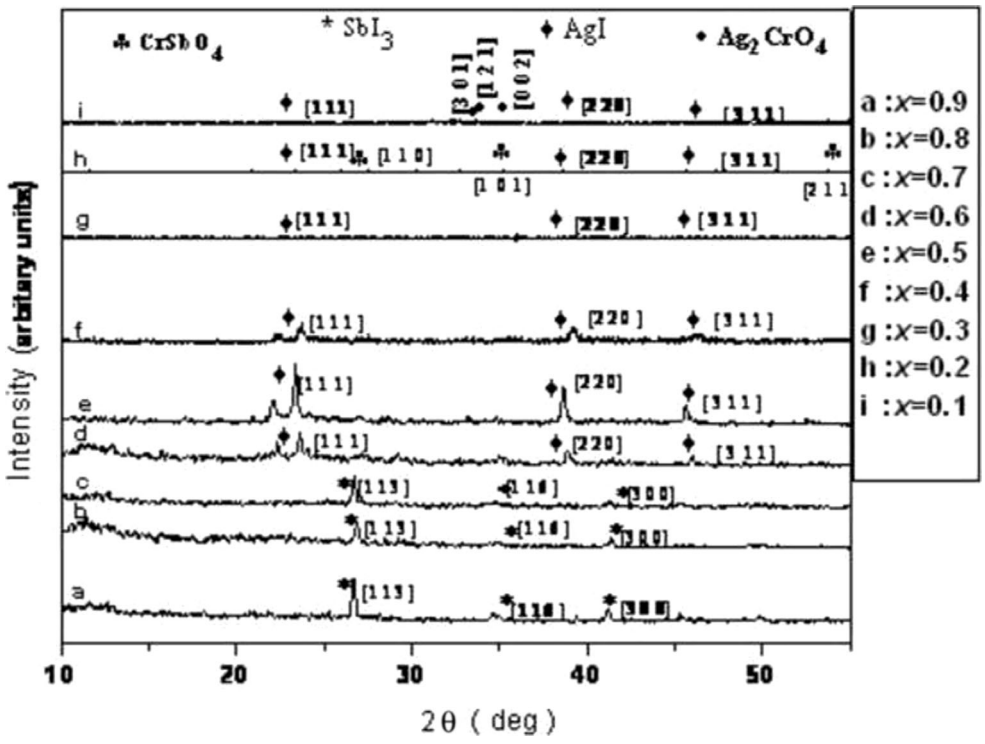

Figure 2. Powder XRD patterns obtained for different compositions of mixed system $(SbI_3)_{1-x}$–$(Ag_2CrO_4)_{1-x}$ $(0{\cdot}1 \leq x \leq 0{\cdot}9)$.

0·4, 0·3, 0·2 and 0·1 mole fractions as a, b, c, d, e, f, g, h and i, respectively are shown in figure 3. Figure 3 suggests that DSC traces recorded over the temperature range 323–460 K exhibit certain interesting features depending on the amounts of reaction products formed in the composition range of $x = 0{\cdot}9 - 0{\cdot}1$ mole fraction. For instance, DSC curve obtained for the particular composition containing $x = 0{\cdot}9$ mole fraction exhibits an endothermic peak at 446 K which corresponds to the melting temperature of SbI_3. In the case of those five different compositions having $x = 0{\cdot}8$, 0·7, 0·6, 0·5 and 0·4 mole fractions, the set of endothermic peaks noticed at 431, 429, 428, 428 and 428 K, respectively confirm the presence of AgI as a new phase formed as a reaction product between SbI_3 and Ag_2CrO_4. Furthermore, it is also evident that those endothermic peaks appearing at 421, 420 and 418 K in the case of compositions containing $x = 0{\cdot}3$, 0·2 and 0·1 mole fractions respectively correspond to the $\beta \rightarrow \alpha$ phase transition of pure AgI occurring at 420 K (Suthanthiraraj *et al* 2001; Suthanthiraraj and Mala 2003; Rivolta *et al* 1988). Thus, the present DSC results are found to be in good agreement with XRD data.

It is interesting to notice from the present DSC data that for compositions corresponding to lower contents of SbI_3 such as $x = 0{\cdot}1$, 0·2 and 0·3 mole fractions, there is an endothermic DSC peak appearing at or near 420 K as revealed by figure 3, due to the $\beta \rightarrow \alpha$ phase transition of AgI. These observations may be attributed to the fact that the addition of SbI_3 into the effective Ag_2O–CrO_3 network i.e. Ag_2CrO_4, would yield a higher concentration of I^- ions compared to the conventional AgI–Ag_2O–CrO_3 framework due to the presence of three I^- ions associated with each Sb^{3+} entity in SbI_3 as against the release of only one I^- ion from each mole of AgI (El Damrawi *et al* 2000). In other words, the present DSC results tend to reveal favourable impact of SbI_3 as an I^- ion source for the formation of crystalline AgI in a variety of compositions of the chosen system.

3.3 *Electrical conductivity and ionic transport number results*

Figure 4 depicts complex impedance plots obtained at different temperatures (298–420 K) for a composition corresponding to $x = 0{\cdot}3$ mole fraction in the mixed system, $(SbI_3)_x$–$(Ag_2CrO_4)_{1-x}$. It is interesting to note from figure 4 that each Nyquist plot consists of a depressed semicircular arc, thus revealing the presence of a bulk resistance (R_b) in parallel connection with a geometric capacitance (C_g) as reported earlier in the case of other solid electrolyte materials (Viswanathan and Suthanthiraraj 1992). According to Armstrong *et al* (1974), ionic single crystals with high conductivity values exhibit semicircular complex impedance plots with simple behaviour intersecting the real axis at two places at or near origin ($\omega = \infty$) and at $R_b(\omega = 0)$ and the difference between these two values corresponds to the bulk resistance of the sample. Similarly, pure AgI (Armstrong *et al* 1972), which exhibits a high ionic conductivity, also

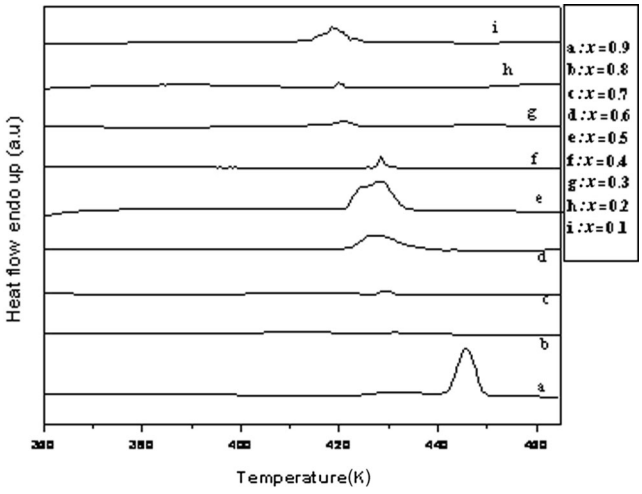

Figure 3. DSC traces for different compositions of mixed system, $(SbI_3)_{0.3}$–$(Ag_2CrO_4)_{0.7}$ ($0.1 \leq x \leq 0.9$).

shows a proper semicircular plot. Generally, fast ionic conductors are polycrystalline in nature with inter-granular grain boundary effects (Hodge *et al* 1976) and could not be represented as single parallel RC equivalent circuit which exhibits complete semicircular arc. Instead, they are represented as series combination of number of parallel RC elements representing distribution of conducting elements of various grains present in the system (Macdonald 1992). Hence, the complex impedance plot of the present solid electrolyte system appears to have two incomplete semicircular arcs including a high frequency one corresponding to bulk resistance (R_b) of the sample in parallel with geometric capacitance, C_g and a low frequency arc representing double layer capacitance, C_{dl}, of the electrode–electrolyte interface (Archer and Armstrong 1980). Actually, the high frequency region shows a portion of a semicircular arc whose centre is depressed below the x axis with an angle of inclination as $\alpha\pi/2$, where 'α' is a measure of breadth of distribution of elements (Jonscher 1978). The low frequency part appears to be the commencement of yet another semicircle inclined with real axis and not fully covered within the frequency range studied. Extrapolation of this plot produces a depressed semicircle as reported earlier (Padmasree *et al* 2005). Hence, from the point of intersection of the semicircular part on the Z'-axis, the corresponding value of R_b was determined by employing the internally incorporated software package with an excellent accuracy, for all the nine different specimens. Subsequently, room temperature electrical conductivity ($\sigma_{298\ K}$) values were estimated from the general relationship

$$\sigma = t/(A^* R_b), \tag{3}$$

where t denotes the thickness of the sample pellet and A its area of cross-section. It is also obvious from figure 4 that the point of intersection on the real axis is shifted towards origin and the diameter of the semicircular arc decreases with increase in temperature and hence the value of bulk resistance (R_b) decreases at elevated temperatures which in turn leads to an increase in the electrical conductivity value with increase in temperature (Suthanthiraraj and Premchand 2004).

The experimentally determined $\sigma_{298\ K}$ values for nine different compositions of the mixed system having $x = 0.9$, 0·8, 0·7, 0·6, 0·5, 0·4, 0·3, 0·2 and 0·1 mole fraction were found to be 3.8×10^{-6}, 2.7×10^{-4}, 1.1×10^{-4}, 4.3×10^{-4}, 3.5×10^{-4}, 4.1×10^{-4}, 3.2×10^{-2}, 4.7×10^{-4} and 3.9×10^{-6} S cm^{-1}, respectively. It is seen from these conductivity (σ) data that the feasibility of realization of typical σ values of the order of 10^{-4} S cm^{-1} in the case of samples containing $x = 0.8$, 0·7, 0·6, 0·5, 0·4 and 0·2 mole fraction may be attributed to the presence of AgI in such compositions (Chandra 1981). The fact that the formation of AgI as one of the constituents in these compositions has already been revealed from XRD and DSC results tend to reconfirm the mechanism of possible ion exchange reactions occurring between SbI_3 and Ag_2CrO_4. Interestingly, the composition containing 0·3 mole fraction of SbI_3 corresponding to $x = 0.3$ mole fraction was found to be the best conducting composition owing to its highest room temperature conductivity of 3.2×10^{-2} S cm^{-1}.

Hence, at the above room temperature, electrical conductivity data appear to indicate that there is a systematic trend in the variation of conductivity of the chosen system probably due to the formation of AgI in the synthesized samples as revealed by the present XRD and DSC results. It is, therefore, expected that similar behaviour would be exhibited by different compositions in their ion-transport properties too as reported in a number of similar mixed systems including xCuI–(100–x) [$2Ag_2O$–$0.7V_2O_5$–$0.3B_2O_3$] (Murugesan *et al* 2008), xCdI$_2$–(100–x)[$2Ag_2O$–($0.7V_2O_5$–$0.3B_2O_3$)] (Padmasree *et al* 2005), CuI–Ag_2O–V_2O_5 (Chandrasekar and Suthanthiraraj 1993), CdI$_2$–Ag_2O–MoO_3 (Suthanthiraraj and Ganeshkumar 2001), PbI$_2$–Ag_2O–V_2O_5, PbI$_2$–Ag_2O–TeO_2 and PbI$_2$–Ag_2O–P_2O_5 (El Damrawi *et al* 2000) etc. According to El Damrawi *et al* (2000), in the case of PbI$_2$–Ag_2O–TeO_2 and PbI$_2$–Ag_2O–P_2O_5 networks, the concentration of iodine ions originating from PbI$_2$ is higher than that originating from similar networks such as AgI–Ag_2O–TeO_2 and AgI–Ag_2O–P_2O_5. Two iodine ions are provided to the tellurite network upon adding one mole PbI$_2$, whereas only one iodine ion could be accommodated when AgI is introduced in the same network. Similarly, in the case of the present system also, three iodine ions are likely to be added to the silver chromate network upon adding one mole of SbI_3, whereas only one iodine ion could be added in the case of AgI–Ag_2CrO_4 network (Durga Rani and Hariharan Durga 1996).

In the case of the new system, viz. $(SbI_3)_x$–$(Ag_2CrO_4)_{1-x}$ ($0.1 \leq x \leq 0.9$)) developed by us, it was also intended to optimize the best conducting composition. Obviously, the addition of SbI_3 into the Ag_2CrO_4 network in terms of varying concentrations does play an important role in determining the conduction mechanism. As the concentration of x (i.e.

mole fraction of SbI_3) increases, the conductivity increases, reaches a maximum value of $3{\cdot}2 \times 10^{-2}$ S cm^{-1} for $x = 0{\cdot}3$ mole fraction and then starts decreasing on further addition of SbI_3. As observed from the XRD results, typical composition having $x = 0{\cdot}3$ mole fraction, was identified to exhibit a disordered nature, whereas crystalline AgI phase is found to exist as reaction product between SbI_3 and Ag_2CrO_4 and was present in compositions corresponding to $x = 0{\cdot}1$, 0·2, 0·4, 05 and 0·6 mole fraction unlike those remaining compositions containing $x = 0{\cdot}7$, 0·8 and 0·9 mole fraction possessing relatively higher concentrations of SbI_3.

Figure 5 depicts plots of log σT *vs* $1/T$ obtained for nine different compositions of the mixed system $(SbI_3)_x$–$(Ag_2CrO_4)_{1-x}$ containing $x = 0{\cdot}9$, 0·8, 0·7, 0·6, 0·5, 0·4, 0·3, 0·2 and 0·1 mole fraction, respectively over the temperature (T) range 298–435 K. Figure 5 appears to suggest the Arrhenius-type of behaviour of temperature-dependent electrical conductivity in view of the fact that the observed σ value is found to increase with increasing temperature in conformity with that of ionic materials (Chandra 1981). In general, the temperature dependence of conductivity (σ) in the case of fast ionic solid may be expressed by the Arrhenius relation (Kawamura and Shimoji 1986)

$$\sigma_{(T)} = (\sigma_0/T)\exp(-E_a/kT), \tag{4}$$

where σ_0 is the pre-exponential factor, E_a, the activation energy for ionic migration within the solid, k, the Boltzmann constant and T the absolute temperature. Accordingly, best fit patterns of all the observed Arrhenius plots shown in figure 5 were drawn with accuracy for the evaluation of relevant activation energy (E_a) data corresponding to individual compositions. As a consequence, the estimated values of activation energies for the set of nine different compositions containing $x = 0{\cdot}9$, 0·8, 0·7, 0·6, 0·5, 0·4, 0·3, 0·2 and 0·1 mole fractions of SbI_3 in the temperature range of 298–403 K were found to be 0·51, 0·4, 0·45, 0·41, 0·3, 0·28, 0·16, 0·26 and 0·46 eV, respectively. From these results, it is clear that highly conducting specimen viz. those corresponding to $x = 0{\cdot}3$ mole fraction, possesses very low activation energies for conduction in good agreement with the observed trend of conductivity among various compositions of the mixed system, SbI_3–Ag_2CrO_4. It is quite interesting to note from figure 5 that in the case of compositions corresponding to $x = 0{\cdot}3$ mole fraction and almost in all compositions, there is an abrupt change in the value of conductivity at around 420 K which may be attributed to the presence of AgI as a constituent phase in these samples in conformity with the present DSC data.

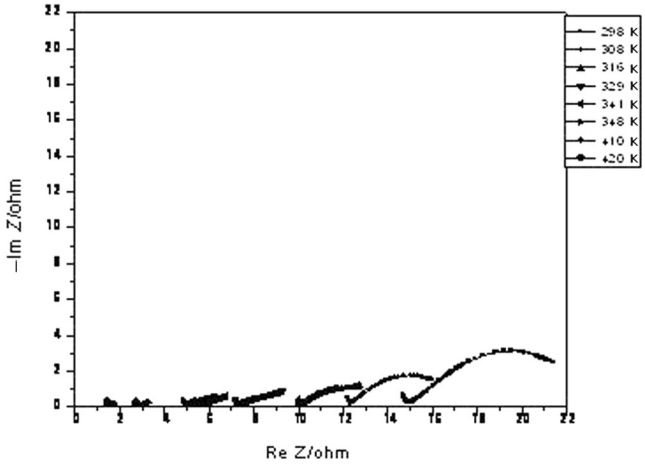

Figure 4. Complex impedance plots obtained for typical composition of mixed system $(SbI_3)_{0{\cdot}3}$–$(Ag_2CrO_4)_{0{\cdot}7}$.

Table 1 presents summary of electrical transport data obtained for the mixed system, $(SbI_3)_x$–$(Ag_2CrO_4)_{1-x}$ (where $x = 0{\cdot}9$, 0·8, 0·7, 0·6, 0·5, 0·4, 0·3, 0·2 and 0·1 mole fractions, respectively), in terms of the measured values of room temperature electrical conductivity ($\sigma_{298\ K}$) along with silver ionic transport number ($t_{Ag}{}^+$) values. It is apparent from table 1 that silver ionic transport number ($t_{Ag}{}^+$) data obtained for the system, $(SbI_3)_x$–$(Ag_2CrO_4)_{1-x}$ from EMF technique at room temperature include 0·92, 0·93, 0·93, 0·94, 0·94, 0·95, 0·99, 0·96 and 0·94 for $x = 0{\cdot}9$, 0·8, 0·7, 0·6, 0·5, 0·4, 0·3, 0·2 and 0·1 mole fraction, respectively. It is evident from table 1 that silver ionic transport number ($t_{Ag}{}^+$) data obtained for various compositions lie in the range of 0·92–0·99, thus indicating the occurrence of silver ionic conduction in the mixed system, SbI_3–Ag_2CrO_4 and that for the highly conducting composition having $x = 0{\cdot}3$ mole fraction, it is almost unity (i.e. 0·99). These features clearly show that major contribution to the total electrical conductivity in the chosen system may be due to silver ions only as in the case of similar systems such as AgI–Ag_2CrO_4 (Durga Rani and Hariharan 1996), CuI–Ag_2MoO_4 (Viswanathan and Suthanthiraraj 1992), PbI_2–Ag_2O–WO_3 (Suthanthiraraj and Vinod Mathew 2005), $Cu_{1-x}Ag_xI$–Ag_2O–B_2O_3 (Suthanthiraraj *et al* 2001), CuI–Ag_3AsO_4 (Rivolta *et al* 1988), CuI–Ag_2WO_4 and CuI–Ag_2CrO_4 (Suthanthiraraj and Premchand 2004). It is evident from the present XRD and DSC data that AgI exist as one of the constituent phases in the case of compositions having $x = 0{\cdot}1$, 0·2 and 0·3 mole fractions. Pure AgI was reported to possess an electronic transference number at around 0·08±0·02 at 293 K (Hoshino and Shimoji 1974), thus suggesting an ionic transference number of 0·92±0·02 at ambient conditions. During the present investigation, the observed silver ionic transport number data for various compositions lie in the region of 0·92–0·99. The fact that the best conducting composition having $x = 0{\cdot}3$ exhibits the highest silver ionic transport number (t_{Ag+}) of 0·99 implying that in addition to AgI, the presence of a probable silver ion-based disordered phase may also give rise to the appreciably high silver ionic transport number in this particular specimen. In other words, Ag^+ ions are found to be effective mobile species in most of the compositions synthesized during the present work.

3.4 *Conductivity spectra*

Figure 6 depicts conductivity spectra (i.e. log σ *vs* log ω plots) observed for the best conducting composition,

Table 1. Summary of electrical transport data obtained for the system, $(SbI_3)_x$–$(Ag_2CrO_4)_{1-x}$.

Composition, x (Mole fraction)	Room temperature conductivity, $\sigma_{298\ K}$ (S cm^{-1})	Silver ionic transport number data (EMF method)		Activation energy, E_a (eV)
		OCV (E_t) (mV)	t_{Ag^+}	
0·9	$3{\cdot}8 \times 10^{-6}$	632·0	0·92	0·51
0·8	$2{\cdot}7 \times 10^{-4}$	638·9	0·93	0·40
0·7	$1{\cdot}1 \times 10^{-4}$	638·9	0·93	0·45
0·6	$4{\cdot}3 \times 10^{-4}$	645·7	0·94	0·41
0·5	$3{\cdot}5 \times 10^{-4}$	645·7	0·94	0·30
0·4	$4{\cdot}1 \times 10^{-4}$	652·6	0·95	0·28
0·3*	$3{\cdot}2 \times 10^{-2}$	680·1	0·99	0·16
0·2	$4{\cdot}7 \times 10^{-4}$	659·5	0·96	0·26
0·1	$3{\cdot}9 \times 10^{-6}$	645·7	0·94	0·46

*Best conducting composition.

$(SbI_3)_{0.3}$–$(Ag_2CrO_4)_{0.7}$, at four different temperatures in the range of 298–388 K. The observed conductivity spectra comprised of three regions viz. low-frequency region, a frequency-independent plateau region corresponding to d.c. conductivity in addition to the high frequency dispersion region, indicating to obey Jonscher's universal power law (Baskaran *et al* 1997) as in the case of other fast ionic conductors

$$\sigma(\omega) = \sigma(0) + A\omega^n. \tag{5}$$

The values of the fitting parameters A, n and σ (0) estimated at four different temperatures viz. 298, 316, 348 and 388 K are presented in table 2. Knowing the values of n, A and σ (0), the values of hopping rate of the mobile species, ω_p, were calculated (Radhakrishnan and Chowdari 1987) using the relation

$$\omega_p = [\sigma(0)/A]^{1/n}, \tag{6}$$

i.e. at a point where $\sigma(\omega) = 2\sigma(0)$ and ω_p has been identified as the hopping rate of Ag^+ ions. It may be seen from table 2 that ω_p shifts to higher frequencies as the temperature is increased from 298 to 388 K. The fitting parameters A, n and $\sigma(0)$ have been found to be strongly temperature-dependent i.e. 'A' values increase with increase of temperature while 'n' values decrease with increasing temperature, whereas $\sigma(0)$ values estimated from the conductivity spectral analysis are in good agreement with those calculated from impedance plots as in the case of other silver ion conducting solid electrolytes.

4. Conduction mechanism

It is clear that $(SbI_3)_x$–$(Ag_2CrO_4)_{1-x}$, material acts as a fast ionic conductor with properties similar to that of silver ion

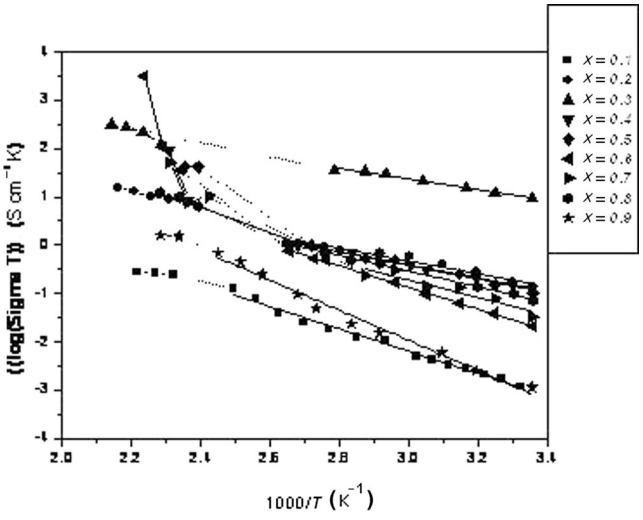

Figure 5. Arrhenius plots of electrical conductivity obtained for composition of mixed system $(SbI_3)_x$–$(Ag_2CrO_4)_{1-x}$ ($0{\cdot}1 \leq x \leq 0{\cdot}9$).

conducting solid electrolytes reported in the mixed system, AgI–Ag_2CrO_4 (Durga Rani and Hariharan 1996). It is well known that fast ionic transport is favoured by any sublattice comprising a large and highly polarizable anion, e.g., I^-, in combination with a relatively small and polarizable metal ion, e.g., Ag^+ (Baskaran 2002). The formation of highly conducting composition in the present system may be explained on the basis of hard and soft acids and bases (HSAB) principle proposed by Pearson (1963). The HSAB rule states that soft acids prefer to bind to soft or polarizable bases and those hard acids would prefer to bind to hard or non-polarizable bases as a result of various degrees of ionic and covalent bonding. It is therefore possible that silver iodide is formed during the ion exchange reaction between antimony iodide and the silver oxy-salt, Ag_2CrO_4 as in an acid–base reaction

$$A:+:B \rightarrow A:B, \tag{7}$$

Table 2. Values of temperature-dependent electrical conductivity parameters for the sample, $(SbI_3)_{0.3}$–$(Ag_2CrO_4)_{0.7}$.

Temperature (K)	n	A (S cm^{-1} rad^{-n})	$\sigma(0)$(S cm^{-1})	Hopping rate, $\omega_p = [\sigma(0)/A]^{1/n}$ (rad s^{-1})
298	0·49	8×10^{-7}	$3{\cdot}2 \times 10^{-2}$	$2{\cdot}1 \times 10^{9}$
316	0·4	5×10^{-6}	$4{\cdot}7 \times 10^{-2}$	1×10^{10}
348	0·39	$5{\cdot}4 \times 10^{-6}$	$9{\cdot}8 \times 10^{-2}$	$2{\cdot}8 \times 10^{10}$
388	0·24	4×10^{-5}	$9{\cdot}9 \times 10^{-2}$	$7{\cdot}9 \times 10^{13}$

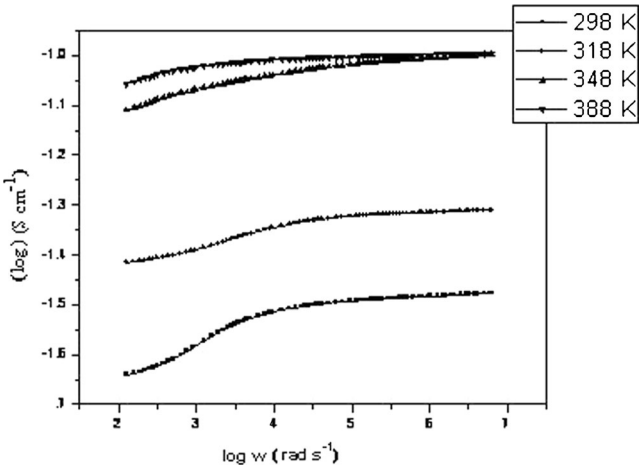

Figure 6. Conductivity spectra for composition $(SbI_3)_{0.3}$–$(Ag_2CrO_4)_{0.7}$.

where the reaction product A:B is known as coordination compound or an acid–base complex (Viswanathan and Suthanthiraraj 1992). According to the HSAB concept, hard acids prefer binding to the hard bases to give ionic complexes, whereas the soft acids prefer binding to soft bases to give covalent complexes. The large electronegativity differences between hard acids and hard bases give rise to strong ionic interactions. Their small sizes allow the acid and base to get close enough together so that the ionic interaction is quite strong. The electronegativities of soft acids and soft bases are almost similar and hence have less ionic interactions. i.e. interactions between them are more covalent because their electron clouds are polarizable. Thus, a strong interaction occurs between large metal ions with high electronegativity and the most polarizable bases. Since SbI_3 is an intermediate acid, the soft acid Ag^+ and soft base I^- prefer to form AgI clusters in agreement with the above principle whenever the concentration (in terms of mol%) of SbI_3 present in the mixture during the melting process is sufficient. During the melting process, initially Ag_2O may decompose into metallic silver and oxygen. Metallic silver released from Ag_2O could possibly be involved in the exchange reaction with SbI_3, thus forming AgI. Similar ion exchange reactions have been reported by earlier researchers as well (Padmasree and Kanchan 2006; Suthanthiraraj and Sankaran 2012; Suthanthiraraj and Sarumathi 2012).

Usually, the acid-base combination would result in the formation of a complex ion or in an electrically neutral compound. Silver iodide may be assumed to be a Lewis acid–base combination. Hence, AgI will be formed while SbI_3 is melted together with Ag_2CrO_4 in accordance with the HSAB principle. The fact that CrO_3 glass former is a strong oxidant and that Cr^{6+} entity in Ag_2CrO_4 is also strongly oxidizing may favourably influence the incorporation of SbI_3 in building up an appropriate structural network wherein the presence of larger I^- ions would give rise to an ion exchange reaction occurring between I^-, Sb^{3+} and Ag^+ ions as in the case of Lewis acid–base type of reactions. Owing to such a specific exchange mechanism, there is a feasibility of an apparent substitution of Ag bonded to non-bridging oxygen (NBO) sites by Sb in order to form AgI phase, thus releasing Ag^+ ions which would become available for an enhanced ionic conductivity of the present fast ion conducting system. Addition of metal oxide to a glass former usually involves incorporation of oxygen into the macromolecular chain formed by the network former, thereby introducing ionic bonds into the glass. Such incorporation depends mainly on the coordination chemistry of the glass former element. When the ratio of glass modifier to glass former content increases, a larger number of oxygen bridges are likely to be broken and as a consequence of the enhanced number of nonbridging oxygen atoms (NBOs), the average length of the macromolecular chain decreases. In fact, an increase in the content of Ag_2O was reported to give rise to breakage of bonds, thereby facilitating an easy migration of the conducting species viz. Ag^+ ions (Sarma and Radhakrishna 1991).

5. Conclusions

The physic-chemical characterization of $(SbI_3)_x$–$(Ag_2CrO_4)_{1-x}$ mixed system has indicated that a typical composition viz. $(SbI_3)_{0.3}$–$(Ag_2CrO_4)_{0.7}$ would exhibit an appreciably high silver ion conductivity of $3{\cdot}2 \times 10^{-2}$ S cm^{-1} at 298 K with an activation energy value of 0·16 eV. XRD and DSC analyses have confirmed the occurrence of an exchange reaction between SbI_3 and Ag_2CrO_4, which could be accounted for the observed fast ionic transport owing to the formation of AgI within the disordered network as revealed by thermal analysis.

References

Archer W I and Armstrong R D 1980 *Electrochim. Acta* **25** 1689

Armstrong R D, Dickinson T and Willis P M 1974 *Electroanal Chem. Interf. Electrochem.* **53** 389

Armstrong R D, Dickinson T and Whitfield R 1972 *J. Electroanal. Chem.* **39** 257

Baskaran N, Govindaraj G and Narayanasamy A 1997 *Solid State Ionics* **98** 217

Baskaran N 2002 *J. Appl. Phys.* **92** 825

Bhattacharya S and Ghosh A 2005 *Solid State Ionics* **176** 1243

Biendicho J J, West A R 2012 *Solid State Ionics* **226** 41

Boukamp B A 1986 *Solid State Ionics* **18–19** 136

Boukamp B A 2000 *Solid State Ionics* **136–137** 75

Boukamp B A 2004 *Solid State Ionics* **169** 65

Chandra S 1981 *Superionic solids—Principles and applications* (New York: North Holland Publishing Company) p. 17

Chandrasekar V G and Suthanthiraraj S A 1993 *J. Mat. Sci.* **28** 4043

Dalvi A, Awasthi A M, Bharadwaj S and Shahi K 2005 *Phys. Chem. Solids* **66** 783

Durga Rani A N and Hariharan K 1996 *Mater. Chem. Phys.* **43** 243

El Damrawi G, Hassan A K and Doweidar H 2000 *Physica B* **291** 34

Hodge I M, Ingram M D and West A R 1976 *J. Electroanal. Chem.* **74** 125

Hoshino H and Shimoji M 1974 *J. Phys. Chem. Solids* **35** 321

Hull S, Keen D A, Sivia D S and Berastegui P 2002 *J. Solid State Chem.* **165** 363

JCDPS File No-740456

JCDPS File No-780641

JCDPS File No-720858

JCPDS File No-351288

Jonscher A K 1978 *J. Mat. Sci.* **13** 553

Kanchan D K, Padmasree K P and Panchal H R 2004 *Ceram. Intern.* **30** 1655

Kawamura J and Shimoji M 1986 *J. Non-Cryst Solids* **88** 281

Macdonald J R 1973 *J. Chem. Phys.* **58** 4982

Macdonald J R 1974 *J. Chem. Phys.* **61** 3977

Macdonald J R 1987 *Impedance spectroscopy*. Wiley-Interscience, New York, p. 206

Macdonald J R 1992 *Ann. Biomed. Eng.* **20** 289

Minami T 1983 *J. Non-Cryst Solids* **56** 15

Metikos M, Hukovic and Grubac Z 2003 *J. Electroanal.Chem.* **556** 167

Murugesan S, Wijayasinghe A and Bergman B 2008 *J. Non-Cryst. Solids* **354** 1066

Nowinski J L, Ksiezopolski M K, Garbarczyk J E and Wasiucionek M 2007 *J. Power Sources* **173** 811

Padmasree K P, Kanchan D K, Panchala H R, Awasthi A M and Bharadwaj S 2005 *Solid State Commun.* **136** 102

Padmasree K P and Kanchan D K 2006 *J. Non-Cryst. Solids* **352** 3841

Patnaik J R G and Sunandana C S 1998 *J. Phys. Chem. Solids* **59** 1059

Pearson R G 1963 *J. Am. Chem. Soc.* **85** 3533

Pyung-An Ahn, Eui-Chol Shin, Gye-Rok Kim and Jong-Sook L 2011 *J. Korean Ceram. Soc.* **48** 549

Radhakrishnan K and Chowdari B V R 1987 *Solid State Ionics* **24** 225

Renard C, Coquet G and Bychkov E 2002 Solid State Ionics **154–155** 749

Rivolta B, Bonino F and Scrosati B 1988 *Mater. Chem. Phys.* **19** 557

Sarma R V G K and Radhakrishna S 1991 *J. Solid State Chem.* **91** 204

Saito T, Tatshumisago M and Minami T 1993 *Solid State Ionics* **61** 285

Suthanthiraraj S A and Daniel Premchand Y 2004 *J. Solid State Chem.* **177** 4126

Suthanthiraraj S A and Ganeshkumar A C 2001 *Indian J. Eng. & Mater. Sci.* **8** 352

Suthanthiraraj S A and Mala R 2003 *J. Solid State Electrochem.* **7** 232

Suthanthiraraj S A, Murugesan S and Maruthamuthu P 2001 *Solid State Ionics* **143** 413

Suthanthiraraj S A and Vinod Mathew 2005 *Indian J. Phys.* **79** 753

Suthanthiraraj S A and Sankaran V S 2012 Ionics doi:10.1007/s11581-012-0804-y

Suthanthiraraj S A and Sarumathi R 2012 Ionics doi:10.1007/s11581-012-0826-y

Veeranna Gowda V C and Anavekar R V 2007 *J. Mat. Sci.* **42** 3816

Viswanathan A and Suthanthiraraj S A 1992 *Solid State Ionics* **58** 89

Viswanathan A and Suthanthiraraj S A 1993 *Mater. Res. Bull.* **28** 821